Heterogeneous electro-Fenton treatment of chemotherapeutic drug busulfan using magnetic nanocomposites as catalyst

Şule Camcıoğlu, Baran Özyurt, Nihal Oturan, David Portehault, Clément Trellu, Mehmet Oturan

Heterogeneous electro-Fenton treatment of chemotherapeutic drug Busulfan using magnetic nanocomposites as catalyst

Şule Camcıoğlu[1,2], Baran Özyurt[1,2], Nihal Oturan[2], David Portehault[3], Clément Trellu[2], Mehmet A. Oturan[2,*]

[1] Ankara University, Faculty of Engineering, Department of Chemical Engineering, 06100 Tandogan, Ankara, Turkey

[2] Université Gustave Eiffel, Laboratoire Géomatériaux et Environnement EA 4508, 77454, Marne-la-Vallée, Cedex 2, France

[3] Sorbonne Université, CNRS, Laboratoire de Chimie de la Matière Condensée de Paris (CMCP), 4 place Jussieu, Paris, France

* Corresponding author Email: Mehmet.oturan@univ-eiffel.fr

ABSTRACT

The rapid and efficient mineralization of the chemotherapeutic drug busulfan (BSF) as the target pollutant has been investigated for the first time by three different heterogeneous EF systems that were constructed to maintain the continuous electro-generation of H_2O_2 and $^{\bullet}OH$ consisting of: i) a multifunctional carbon felt (CF) based cathode composed of reduced graphene oxide (rGO), iron oxide nanoparticles and carbon black (CB) (rGO-Fe_3O_4/CB@CF), ii) rGO modified cathode (rGO/CB@CF) and rGO supported Fe_3O_4 (rGO-Fe_3O_4) catalyst, iii) rGO modified cathode (rGO/CB@CF) and multi walled carbon nanotube supported Fe_3O_4 (MWCNT-Fe_3O_4) catalyst. The effects of main variables, including the catalyst amount, applied current and initial pH were investigated. Based on the results, H_2O_2 was produced by oxygen reduction reaction (ORR) on the liquid-solid interface of both fabricated cathodes. $^{\bullet}OH$ was generated by the reaction of H_2O_2 with the active site of $\equiv Fe^{II}$ on the surface of the multifunctional cathode and heterogeneous EF catalysts. Utilizing carbon materials with high conductivity, the redox cycling between $\equiv Fe^{II}$ and $\equiv Fe^{III}$ was effectively facilitated and therefore promoted the performance of the process. The results demonstrated almost complete mineralization of BSF through the

heterogeneous systems over a wide applicable pH range. According to the reusability and stability tests, multifunctional cathode exhibited outstanding performance after five consecutive cycles which is promising for the efficient mineralization of refractory organic pollutants. Moreover, intermediates products of BSF oxidation were identified and a plausible oxidation pathway was proposed. Therefore, this study demonstrates efficient and stable cathodes and catalysts for the efficient treatment of an anticancer active substance.

Key words: Heterogeneous electro-Fenton, Electrochemical advanced oxidation, Cytotoxic, Magnetic nanocomposite, Reduced graphene oxide, Carbon nanotubes

1. INTRODUCTION

The increasing use of drugs for cancer treatment and their poor metabolism in the human body result in high concentrations of these drugs and/or their metabolites in hospital and municipal wastewaters (Kanjal et al., 2020; Kulaksız et al., 2022). Effluents from wastewater treatment plants are considered to be the main source of release of these drugs and their metabolites into water resources (Zhang et al., 2013; Ioannou-Ttofa and Fatta-Kassinos, 2020; Siedlecka, 2020). Although effluent concentration of chemotherapeutic drugs are generally at ng L^{-1} level, they have been shown to have cytotoxic, genotoxic, mutagenic, endocrine disrupting and/or teratogenic effects in aquatic and terrestrial ecosystems (Li et al., 2016; Yang et al., 2020a). Recognition of the presence of these drugs has prompted research into potential methods for removing them from water bodies, including activated sludge aerobic bioreactors (Kosjek et al., 2018), photocatalytic degradation (Calza et al., 2014; González-Burciaga et al., 2022), chlorination (Roig et al., 2014), UV/H_2O_2, UV/Fe^{2+}/H_2O_2 and UV/TiO_2 processes (González-Burciaga et al., 2021), ozonation (Li et al., 2016), Fenton reagent (Governo et al., 2017), photo-Fenton (Cavalcante et al., 2013), anodic oxidation (Barışçı et al., 2018) and EF (Kulaksız et al., 2022; Yang et al., 2019).

As one of the most widely studied electrochemical advanced oxidation processes (EAOPs), electro-Fenton (EF) is considered as a promising method owing to high oxidation/mineralization efficiency against recalcitrant organic pollutants, low cost and simple operating conditions (Camcioglu et al., 2022; Martínez-Huitle et al., 2022). In

this process, H_2O_2 is electrochemically generated on-site by the two-electron oxygen reduction reaction (ORR) at the carbonaceous cathode (Eq.(1)) (Barhoumi et al., 2017). Formed H_2O_2 is decomposed by the externally added catalyst (Fe^{2+}) promoting the continuous generation of homogeneous $^{\bullet}OH$ via Fenton reaction (Eq.(2)) (Zhou et al., 2018). Fe^{2+} consumed in Fenton reaction is regenerated electrochemically of Fe^{3+} at the cathode (Eq.(3)) ensuring continuous formation of $^{\bullet}OH$ (Yang et al., 2019, 2020b).

$$O_2 + 2H^+ + 2e^- \rightarrow H_2O_2 \quad (1)$$

$$H_2O_2 + Fe^{2+} \rightarrow Fe^{3+} + OH^- + {}^{\bullet}OH \quad (2)$$

$$Fe^{3+} + e^- \rightarrow Fe^{2+} \quad (3)$$

However, some challenges are encountered during the application of homogeneous EF such as low pH range (pH 2.5-3.5) requirement for optimal process efficiency (Li et al., 2009; Wang et al., 2013; Chen et al., 2015). Further, the catalyst Fe^{2+} in homogeneous EF has to be precipitated before discharge, which prevents the reusability and recyclability of the catalyst in continuous processes and also generates a sludge that requires a secondary process to be disposed (Ganiyu et al., 2018; Poza-Nogueiras et al., 2018; Nidheesh et al., 2023b).

To overcome these drawbacks, the heterogeneous EF process, which uses a solid catalyst for the decomposition of H_2O_2 to $^{\bullet}OH$, has been developed (Gopinath et al., 2022). Heterogeneous EF process offers solutions such as preventing the generation and disposal of iron-rich sludge, widening working pH range, catalyst recovery and reusability by utilizing heterogeneous catalysts and functionalized cathodes with enhanced durability, high conductivity, and large surface area (Ganiyu et al., 2018; Nidheesh et al., 2022).

It is widely accepted that heterogeneous EF catalysis may fit the Haber-Weiss mechanism, which is summarized by reactions in Eqs (4-9).

$$\equiv Fe^{III} - OH + e^- \rightarrow \equiv Fe^{II} - OH \quad (4)$$

$$\equiv Fe^{III} - OH + H_2O_2 \leftrightarrow \equiv Fe^{III} - OH(H_2O_2)_s \quad (5)$$

$$\equiv Fe^{III} - OH(H_2O_2)_s \rightarrow \equiv Fe^{II} - OH(HO_2^{\bullet})_s + H^+ \quad (6)$$

$$\equiv Fe^{II} - OH(HO_2^{\bullet})_s \rightarrow \equiv Fe^{II} - OH + HO_2^{\bullet} + H^+ \quad (7)$$

$$\equiv Fe^{II} - OH + H_2O_2 \rightarrow \equiv Fe^{III} - OH + {}^{\bullet}OH + OH^- \quad (8)$$

$${}^{\bullet}OH + \text{organic pollutants} \rightarrow \text{oxidation intermediates} \rightarrow CO_2 + H_2O \quad (9)$$

When current is applied to the system, partial reduction of ≡Fe^{III}—OH to ≡Fe^{II}—OH by gaining one electron at the surface of the iron containing heterogeneous catalyst (Eq.(4)) accompanied with generation of H_2O_2 in large amounts at the cathode (Eq.(1)) initiates the mechanism (Wang et al., 2013). H_2O_2 interacts with the negatively charged catalyst surface, to produce a precursor surface complex (≡Fe^{III}—OH(H_2O_2)) representing the surface properties of H_2O_2 within the inner and outer surface of the cathode matrix (Eq.(5)). Further, surface H_2O_2 complex may be subjected to a reversible ground-state electron transfer from the ligand to metal (Eq.(6)) and the successor complex then would be deactivated through Eq. (7) to form $HO_2^{\bullet}$ and ≡Fe^{II}—OH (Zhao et al., 2012). It is obvious that the reaction in Eq.(6) is particularly active in alkaline media since the protons (H^+) can instantaneously react with hydroxyl ions (OH^-) to enhance the rate of reaction (Zhao et al., 2012). The reduced iron sites (Fe^{II}–OH) then again react with H_2O_2 (Eq.(8)) to regenerate Fe^{III}–OH sites and form ${}^{\bullet}OH$ that can oxidize the organic compounds until complete mineralization to CO_2 and H_2O (Eq.(9)) (Zhao et al., 2012).

Iron oxides are the pillars of nanomaterials used in water treatment due to their natural abundance, and relatively low toxicity towards receiving environments (Rusevova et al., 2012; Xu and Wang, 2012; Ganiyu et al., 2022). Fe_3O_4 is the most basic magnetic iron oxide with inverse cubic spinel lattice structure. Fe_3O_4 consists of two irons sub-lattice including a tetrahedral coordination filled by Fe^{III} and an octahedral coordination occupied by both Fe^{II} and Fe^{III} (Ganiyu et al., 2022). The co-existence of Fe^{II} and Fe^{III} increases the catalytic decomposition of H_2O_2 to form strong oxidizing agent ${}^{\bullet}OH$ (Xue et al., 2009; Gopinath et al., 2022). Although reducing the Fe_3O_4 particle size may increase the catalytic activity, Fe_3O_4 nanoparticles tend to agglomerate and the surface area is reduced (Gao et al., 2007). To overcome this problem, several studies are carried out on the support of Fe_3O_4 nanoparticles on solids such as bentonite, alginate, zeolite, alumina, chitosan and carbon nanotube (Cleveland et al., 2014; Zhou et al., 2014; Yu et al., 2015), porous carbon-based matrices (Chen et al., 2023), activated carbon (Zhang et al., 2014) and graphene oxide (Hua et al., 2014; Zubir et al., 2015).

In order to eliminate the necessities on the recoverability of the catalyst as well as the limitations of pH range, heterogeneous EF using a graphene modified-Fe_3O_4 doped cathode can be considered. Such a cathode can yield both higher H_2O_2 production and its conversion to hydroxyl radical ($^{\bullet}OH$) efficiency and therefore can be considered as a promising approach (Scaria and Nidheesh, 2022; Martínez-Huitle et al., 2023; Nidheesh et al., 2023a;). This Fe_3O_4 functionalized-graphene supported cathode serves dual purpose as it effectively generates H_2O_2 and therefore $^{\bullet}OH$ via the electrochemical reduction of O_2 and in-situ activation of H_2O_2, respectively. As an encouraging alternative, utilization of a graphene modified cathode and a magnetic heterogeneous Fenton catalyst duo was also considered for combining enhanced H_2O_2 production and easy catalyst recovery and reuse in comparison with conventional homogeneous Fenton catalyst.

In this study, we investigated the mineralization of one of the most used chemotherapy drug, the busulfan (BSF) (Houot et al., 2013; Skoglund et al., 2013) solutions by the heterogeneous EF processes. To the best of our knowledge, this constitutes the first work on the efficient removal of BSF from contaminated water. We found only one work from Li et al. (2016) in which degradation of eight chemotherapeutic drug was exanimated by ozonation resulting in lower oxidation kinetics and mineralization rates. Among these chemotherapeutic drugs, BSF was the most recalcitrant to oxidation; only about 20% degradation was achieved with a 1 mg O_3 mg DOC^{-1} ozonation dose.

The present study reports fast and complete mineralization after 4 h treatments by means of three heterogeneous EF systems. Reduced graphene oxide (rGO) and carbon black (CB) modified carbon felt (CF) cathode (rGO/CB@CF) was fabricated and higher H_2O_2 production efficiency was obtained compared to CF. Heterogeneous Fenton process using multi walled carbon nanotube supported iron oxide (MWCNT-Fe_3O_4) and rGO-Fe_3O_4 catalysts with magnetic properties was fabricated. High efficiencies were achieved for the mineralization of BSF with heterogeneous EF process by using rGO/CB@CF cathode and heterogeneous Fenton catalysts. Fe_3O_4 functionalized-reduced graphene oxide (rGO) modified carbon felt cathode (rGO-Fe_3O_4/CB@CF) was fabricated for simultaneous generation and conversion of H_2O_2 to $^{\bullet}OH$ to avoid the addition of external catalyst. The application of this multifunctional cathode in heterogeneous EF process exhibited remarkable results in terms of

mineralization of BSF. Furthermore, the reaction intermediates formed during the oxidation process, the short-chain carboxylic acids as final by-products before complete mineralization and mineral end-products were identified using HPLC, GC-MS and ion chromatography (IC). These data allowed us to propose a plausible mineralization pathway of BSF by $^{\bullet}OH$ generated in the EF process.

2. MATERIAL AND METHODS

2.1 Chemicals

Details of the chemicals used in this study are provided in Supplementary Information file (SI-Text S1).

2.2 Analytical procedures

The mineralization degree of BSF solutions was determined from their TOC decay measurements on a Shimadzu TOC-V_{CSH} analyzer according to the thermal catalytic oxidation principle. Reproducible TOC values are obtained using the non-purgeable organic carbon method with an accuracy of ± 2%.

The mineralization current efficiency (MCE) was calculated from TOC values using Eq. (10) at given electrolysis time based on complete electrochemical oxidation of BSF (Brillas et al., 2009; Dos Santos et al., 2021):

$$\mathrm{MCE}(\%) = \frac{\mathrm{n\ F\ V_S\ \Delta(TOC)_{exp}}}{4.32\times10^{7}\ \mathrm{m\ I\ t}} \times 100 \qquad (10)$$

Here F is the Faraday constant (96485 C mol^{-1}), V_S is the solution volume (L), $\Delta(TOC)_{exp}$ is the experimental TOC decay (mg L^{-1}), 4.32 × 10^7 is a conversion factor for homogenization of units, m is the number of carbon atoms of BSF, I is applied current (A), t is the electrolysis time (h). n is the number of electrons consumed per mole of target molecule during its mineralization. The number of electrons is 38 for mineralization of BSF to CO_2 and sulfate as given in Eq. (11).

$$\mathrm{C_6H_{14}O_6S_2 + 14H_2O \rightarrow 6CO_2 + 2SO_4^{2-} + 42H^+ + 38e^-} \qquad (11)$$

The specific energy consumption (EC) per unit TOC mass removed for each experiment was calculated by using Eq. (12) (Márquez et al., 2020; Murrieta et al., 2020):

$$\mathrm{EC(kWh(g\ TOC)^{-1}) = \frac{E_{cell}\ I\ t}{V_S\ \Delta(TOC)_{exp}}} \quad (12)$$

where E_{cell} is the mean potential difference of the cell (V).

The concentration of H_2O_2 was measured via the potassium titanium oxalate method as detailed in SI-Text S2.

Short-chain carboxylic acids, inorganic ions and the degradation intermediates formed during treatment were analyzed by HPLC, IC and GC-MS analyses, respectively. The detailed analytical procedures of the methodologies were introduced in SI-Text S2.

2.3 Synthesis, preparation and characterization

Synthesis and characterization of graphene oxide (GO), reduced graphene oxide (rGO), Fe_3O_4, rGO-Fe_3O_4 and MWCNT-Fe_3O_4 composites and preparation of modified cathodes are provided in SI-Text S3.

2.4 Electrolytic system

Heterogeneous EF experiments were performed in a 100 mL undivided cylindrical glass cell with 80 mL aqueous solution containing 0.1 mM target pollutant and 50 mM Na_2SO_4 as supporting electrolyte. BDD (16 cm^2) and modified electrode (8 cm^2) were used as anode and cathode, respectively. Experiments were performed under constant current conditions ranging from 100 mA to 1000 mA. Compressed air bubbling (starting 5 min prior to the experiments) was used to provide saturated oxygen condition in the solution for H2O2 generation. The pH was measured with a CyberScan pH 1500 pH-meter from Eutech Instruments. The electrochemical cell was powered by a Hameg HM8040 triple DC power supply. Samples were taken at pre-set time intervals to evaluate the concentration for degradation and mineralization.

The H_2O_2 electro-generation experiments were performed in an undivided cell (250 mL) in 50 mM Na_2SO_4 solution at room temperature and pH=3. Experiments were performed under 100 mA constant current electrolysis condition. The unmodified and modified carbon felt cathodes and a Pt sheet of the same geometric area (4cm×2cm) were used during these experiments.

3. RESULTS AND DISCUSSION

3.1 Effect of cathode modification on electrochemical H_2O_2 generation

Electrochemical H_2O_2 generation performance and TOC removal rate of different cathodes are given in Fig.1. Compared with the unmodified CF (Fig.1a), H_2O_2 production increased 9.6-fold for CB@CF and 23.4-fold for rGO/CB@CF due to the improved mass transfer kinetics of oxygen. H_2O_2 generation rate of rGO/CB@CF was obtained as 10.96 mg h^{-1} cm^{-2} (10.32 mmol L^{-1} h^{-1}), which was significantly higher than the rate yielded by CB@CF as 4.48 mg h^{-1} cm^{-2} (4.22 mmol L^{-1} h^{-1}). Modification of the carbon black supported carbon felt (CB@CF) and rGO/CB@CF cathodes with the addition of PTFE enable a decrease in the oxygen diffusion resistance (Cui et al., 2021). The higher H_2O_2 production performance of rGO/CB@CF over CB@CF can be explained by the improved hydrophilicity of cathode with rGO addition (Du et al., 2021). Generally, the increased hydrophilicity may further reduce the diffusion resistance of oxygen, resulting in a higher H_2O_2 generation (Le et al., 2015; Yang et al., 2017). However, H_2O_2 accumulation of rGO-Fe_3O_4/CB@CF was found to be decreased in comparison to CB@CF and rGO/CB@CF which means a large amount of electrogenerated H_2O_2 decomposed onsite into $^{\bullet}OH$ in consequence of Fe_3O_4 activation (Cui et al., 2021). Heterogeneous EF performance of the modified cathodes was also determined by comparing TOC mineralization rates (Fig.1b). Mineralization of BSF within 1 h reached 98.2% with rGO/CB@CF and 99.1% with rGO-Fe_3O_4/CB@CF cathode, which was higher than that of CF cathode (81.2%). TOC removal rate of CF cathode was found as the lowest due to the fact that it has a weak performance of ORR to generate H_2O_2. Modification of the cathodes by rGO with high conductivity contributed to the higher H_2O_2 accumulation (Xie et al., 2022) and thus higher TOC mineralization yield. Onsite decomposition of H_2O_2 into $^{\bullet}OH$ on the multifunctional rGO-Fe_3O_4/CB@CF cathode was also confirmed by obtaining a very close mineralization yield in comparison with the rGO/CB@CF cathode and MWCNT-Fe_3O_4 catalyst system.

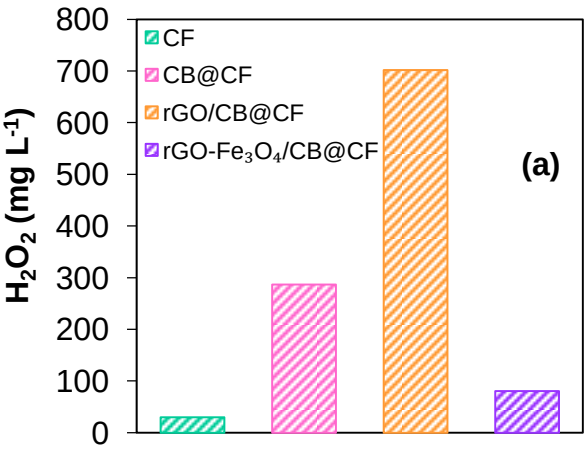

(b)

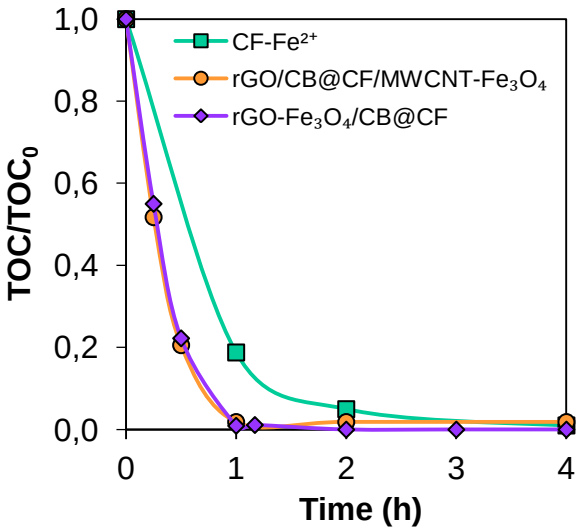

Fig. 1. Electrochemical generation of H_2O_2 **(a)** and TOC removal rate **(b)** using different cathodes at pH = 3 in 50 mM Na_2SO_4 solution. (a): t = 2 h, V = 250 mL, *I* = 100 mA. (b): [BSF] = 0.1 mM, V = 80 mL, *I* = 500 mA. For CF (homogeneous EF): [Fe^{2+}] = 0.1 mM. For heterogeneous EF with rGO/CB@CF cathode/MWCNT-Fe_3O_4 catalyst system: [MWCNT-Fe_3O_4 catalyst] = 0.5 g L^{-1})

LSV (linear sweep voltammetry) and CV (cyclic voltammetry) tests were carried out in the three-electrode cell with the modified cathodes acting as the working electrode. The effect of modifications on the cathode electrochemical activities were discussed in SI-Text S4).

3.2 Characterization of GO, rGO, rGO-Fe_3O_4, MWCNT and MWCNT-Fe_3O_4

UV-VIS spectra of GO, rGO and rGO-Fe_3O_4, FTIR spectra of GO, rGO and rGO-Fe_3O_4, MWCNT, Fe_3O_4 and MWCNT-Fe_3O_4, XRD patterns of rGO, Fe_3O_4 and rGO-Fe_3O_4, TEM images of Fe_3O_4, rGO and rGO-Fe_3O_4 were discussed in SI-Text S5.

3.3 Heterogeneous EF treatment of BSF

3.3.1 The effect of catalyst dosage on mineralization rate of BSF

It is well known that catalyst concentration plays a fundamental role in the efficiency of heterogeneous EF process, since it controls the rate of $^{\bullet}OH$ production. In order to clarify the effect of concentration on mineralization, BSF solutions were treated by varying MWCNT-Fe_3O_4 and rGO-Fe_3O_4 catalyst dosages in the range of 0.2–1.0 g L^{-1} at 100 mA and results are depicted in Figs. 2a-2b. Maximum mineralization efficiency was achieved with 0.2 g L^{-1} of MWCNT-Fe_3O_4 and rGO-Fe_3O_4 resulting in a TOC removal of 89.4% and 96.9%, respectively (Figs. 2a, 2b). It can be seen that mineralization rate of BSF is decreased with increasing catalyst concentration from 0.2 to 1 g L^{-1}. The lowest efficiency was observed at the highest catalyst load (1 g L^{-1}) as 57.05% for MWCNT-Fe_3O_4, whereas it was 0.5 g L^{-1} for rGO-Fe_3O_4 (86.5%). It is reported that the amount of catalyst has a direct effect on the reaction kinetics, since Fe is the catalyst for decomposition of H_2O_2 to form $^{\bullet}OH$. However, when iron oxide is in excess, the scavenging effect of Fe^{2+} is enhanced and results in consumption of $^{\bullet}OH$ through Eq.(13) (Lin et al., 2017; Sadeghi et al., 2019; Chen et al., 2016; Geraldino et al., 2020).

$$Fe^{2+} + {}^{\bullet}OH \rightarrow Fe^{3+} + OH^{-} \quad (13)$$

Therefore, 0.2 g L^{-1} catalyst dosage was chosen as the optimum value for further experiments, considering the mineralization efficiency and catalyst cost.

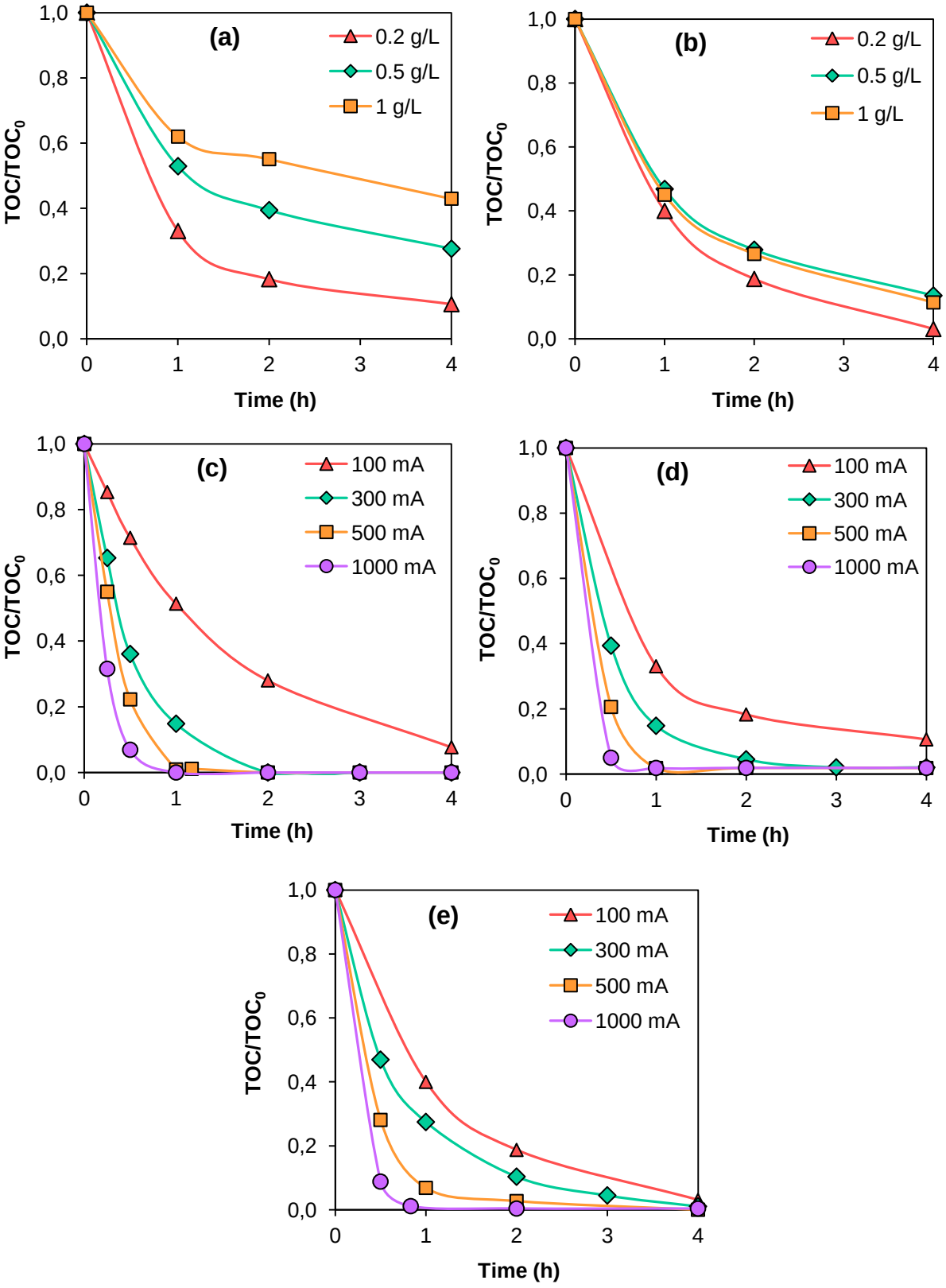
(a)
0.2 g/L
0.5 g/L
1 g/L
TOC/TOC0
Time (h)
(b)
0.2 g/L
0.5 g/L
1 g/L
TOC/TOC0
Time (h)
(c)
100 mA
300 mA
500 mA
1000 mA
TOC/TOC0
Time (h)
(d)
100 mA
300 mA
500 mA
1000 mA
TOC/TOC0
Time (h)
(e)
100 mA
300 mA
500 mA
1000 mA
TOC/TOC0
Time (h)

Fig. 2. TOC decay of 0.1 mM BSF in 50 mM Na_2SO_4 solution as a function of operating parameters: catalyst dosage to rGO/CB@CF cathode/MWCNT-Fe_3O_4 catalyst system at *I* = 100 mA **(a)** and to rGO/CB@CF cathode/rGO-Fe_3O_4 catalyst system at *I* = 100 mA **(b)**; applied current to rGO-Fe_3O_4/CB@CF cathode system **(c)** and to rGO/CB@CF cathode/MWCNT-Fe_3O_4 catalyst system at [MWCNT-Fe_3O_4 catalyst] = 0.2 g L^{-1} **(d)**; applied current to rGO/CB@CF cathode/rGO-Fe_3O_4 catalyst system at [rGO-Fe_3O_4 catalyst] = 0.2 g L^{-1} **(e)**. pH = 3, V = 80 mL, BDD anode

3.3.2 The effect of applied current on mineralization rate of BSF

In order to explore the performance of heterogeneous EF process for complete mineralization of BSF solution, TOC removal experiments were conducted and results are depicted in Fig.2c-2e. Current density is the driving force for electron transfer between the surface of electrodes and the bulk aqueous solution, which controls the amount of H_2O_2 and therefore $^{\bullet}OH$ generation. Fig.2c shows that BSF is completely removed at 1 h of electrolysis at applied current values of 500 and 1000 mA in rGO-Fe_3O_4/CB@CF cathode system, while TOC removal efficiency was 92.3% at applied current of 100 mA at the end of 4 h. When rGO/CB@CF cathode/MWCNT-Fe_3O_4 catalyst system was used, complete mineralization of BSF was achieved at 500 and 1000 mA at 1 h of electrolysis, whereas mineralization rate reached 81.7% and 95.5% at 100 and 300 mA, respectively after 2 h of treatment. For rGO/CB@CF cathode/rGO-Fe_3O_4 catalyst system, TOC mineralization efficiency was increased from 81.3% to 97.3% by increasing current density from 100 to 500 mA after 2 h of electrolysis time. Increasing the applied current further to 1000 mA did not have a considerable effect on the mineralization rate. Considering the results for three systems, TOC removal efficiency increased regularly with increasing applied current density up to 500 mA owing to the promotion of heterogeneous EF in three ways. First, the electro-regeneration of the $\equiv Fe^{II}$ catalyst increases at high currents due to the cathodic reduction of $\equiv Fe^{III}$ (Eq.4), resulting in an increase in the reaction rate. Secondly, anodic oxidation (Eq.(14)) increases with applied current and creates a synergy with the catalyst regeneration at the cathode enhancing EF mineralization of organics in water. Finally, the in situ electro-generation of H_2O_2 (Eq.(1) by the cathodic reduction of oxygen is dependent on the applied current (Muzenda and Arotiba, 2022). However, by increasing the applied current up to 1000 mA, no

significant improvement was observed in BSF mineralization due to the increased rate of side reactions that inhibit the formation of $^{\bullet}OH$ or increase its consumption (Burgos-Castillo et al., 2018; Nidheesh et al., 2023b). The most significant side reactions are evolution of O_2 on the anode surface (Eq.(15) and in the bulk (Eq.(16) which slows down the anodic oxidation rate and the evolution of H_2 at the cathode (Eq.(17), which is in competition with the ORR. (Brillas et al., 2009; Sirés et al., 2014; Berhe et al., 2022; Moratalla et al., 2022).

$$BDD + H_2O \rightarrow BDD(^{\bullet}OH) + H^+ + e^- \quad (14)$$

$$2BDD(^{\bullet}OH) \rightarrow 2BDD + O_2 + 2H^+ + 2e^- \quad (15)$$

$$2H_2O \rightarrow O_2 + 4H^+ + 4e^- \quad (16)$$

$$2H_2O + 2e^- \rightarrow H_2 + 2OH^- \quad (17)$$

Mineralization experiments were also evaluated to estimate the oxidizing power of the heterogeneous EF process with different systems. The degree of TOC removal was the highest for rGO-Fe_3O_4/CB@CF cathode system, except for 100 mA current, which finally reached 92.3% mineralization efficiency at the end of 4 h. Results indicate the ability of Fe_3O_4 functionalized-carbonaceous material (rGO) supported CF cathode to serve dual purpose of electrode as well as the catalyst source in heterogeneous EF system. Compared to the rGO-Fe_3O_4 catalyst system, MWCNT-Fe_3O_4 catalyst system seems to provide a slight improvement in TOC removal efficiency. Since these systems utilize rGO/CB@CF cathode that could produce high quantities of H_2O_2, the slight difference may arise from the catalytic decomposition of H_2O_2 to $^{\bullet}OH$ either by homogeneous Fe^{3+}/Fe^{2+} cycle due to the leaching of iron and surface Fe^{III}/Fe^{II} redox couple (Ganiyu et al., 2018; Görmez et al., 2019). The TOC removal curves obtained at 1000 mA for the three systems are almost identical to those obtained at 500 mA, underlying that no enhancement in mineralization efficiency observed for currents above 500 mA due to the wasting Eqs.(18)-(20) that hinder the increase in H_2O_2 production such as 4-electron reduction of O_2 (Eq.(18), reduction of H_2O_2 at the cathode (Eq.(19)) and dimerization of $^{\bullet}OH$ (Eq.(20)) (Olvera-Vargas et al., 2022; Sopaj et al., 2020).

$$O_2 + 4H^+ + 4e^- \rightarrow 2H_2O \quad (18)$$

$$H_2O_2 + 2H^+ + 2e^- \rightarrow 2H_2O \quad (19)$$

$$2^{\bullet}OH \rightarrow H_2O_2 \quad (20)$$

3.3.3 Efficiency of different systems on mineralization of BSF solution

The results presented in Fig.SI-4 are obtained from corresponding mineralization data of the Fig.2c-2e. Fig.SI-4 depicts the evolution of MCE for applied current values ranging from 100 to 1000 mA during the mineralization process of BSF solution. As seen from this figure, MCE values are relatively high for three systems at low currents and early stage of electrolysis which is an indicator of rapid mineralization of organic intermediates by the action of $^{\bullet}OH$/BDD($^{\bullet}OH$). MCE values then kept diminishing with increasing current until the end of 4 h treatment. This can be explained by the production of hardly oxidizable by-products, such as short-chain carboxylic acids, and the reduction of organic matter concentration in the solution resulting in mass transport limitation to BDD anode (Yang et al., 2020b). On the other hand, low MCE values for high currents can be related to acceleration of parasitic reactions consuming $^{\bullet}OH$, mainly oxidation of BDD($^{\bullet}OH$) to O_2 at the anode surface (Eq.(15)), dimerization of $^{\bullet}OH$ to H_2O_2 (Eq.(20), as well as the wasting of $^{\bullet}OH$ by Fe^{2+} (Eq.(13)) and H_2O_2 (Eq.(21)) (Barhoumi et al., 2017), and particularly the evolution of H_2 at the cathode (Eq.(17)) which competes with the formation of H_2O_2 (Eq.(1)) as well as the evolution of O_2 at the anode (Eq.(16) (Lin et al., 2017). At higher organic matter concentration, when oxidizing radicals can more easily encounter organic molecules, the role of parasitic reactions is less relevant (Brillas and Martínez-Huitle, 2015; Coria et al., 2018).

$$H_2O_2 + {}^{\bullet}OH \rightarrow HO_2^{\bullet} + H_2O \quad (21)$$

In the EAOPs, high currents could generally improve the mineralization efficiency but at the same time lead to low MCE because of the side and wasting reactions in addition of quick formation of hardly oxidizable intermediates such as carboxylic acids (Yang et al., 2020a). Therefore, EC as one of the important parameters will be taken into consideration for comparison of mineralization performance. As can be seen from Fig.SI-5, decay of MCE is generally expected to be associated with an increase in EC per unit mass of TOC (Feng et al., 2023). The results given in Fig.SI-5

show that higher currents and longer electrolysis times result in high EC. This highlights that a compromise between high efficiency and low cost is required. Taking into account of the mineralization rate and energy efficiency, the current value of 500 mA seems to be the best condition for the three systems as total mineralization can be reached at a medium cost. EC results showed that systems with cathode and catalyst completely prepared with rGO had relatively lower EC due to the enhanced electrical conductivity of rGO.

3.3.4 The effect of initial pH on mineralization rate of BSF

The most important superiority of heterogeneous EF over its homogeneous equivalent, which performs significantly low efficiency when working outside the pH range 2.5-3.5, is that it can be operated over a wide pH range (Hien et al., 2022). The effect of pH (3-9) on the mineralization performance of the as-prepared cathodes and catalysts was discussed in SI-Text S6).

3.4 Identification and evolution of carboxylic acids and inorganic ions with heterogeneous EF process

Treatment of organic pollutants by electrochemical advanced oxidation processes generally leads to the generation of short-chain carboxylic acids as the last intermediates of the mineralization process before transformation into CO_2, H_2O and inorganic ions (Camcioglu et al., 2022; Mbaye et al., 2022). Formation and evolution of different carboxylic acids generated during the oxidative degradation of BSF by heterogeneous EF process with rGO-Fe_3O_4/CB@CF cathode is given in Fig.3a. Four distinctive and well-defined peaks corresponding to oxalic, glyoxylic, pyruvic and formic acids were shown on the HPLC chromatograms at retention time of 6.64, 9.17, 11.28 and 13.55 min and quantified with different accumulation trends. Oxalic acid is generated from the beginning of the process and increased gradually until reaching the maximum peak concentration (0.088 mM) at 120 min. Then, its concentration progressively decreased but not completely disappeared at the end of 6 h treatment, since this acid is known to be resistant to oxidation by $^{\bullet}OH$ and responsible for the residual TOC at the end of treatment (Diaw et al., 2020). Glyoxylic acid reached its maximum concentration of 0.042 mM after 90 min of electrolysis and then completely mineralized at 300 min. For formic acid, maximum concentration of 0.023 mM was

attained after 20 min electrolysis and this acid disappeared after 120 min. Pyruvic acid was only detected at trace amounts along electrolysis.

Inorganic ion formed during the mineralization of 0.1 mM BSF solution were identified and quantified by ion chromatography. BSF contains two S atoms in its initial structure which expected to be mineralized into inorganic ion SO_4^{2-} upon bond cleavage of BSF molecule. The evolution of SO_4^{2-} ion generated during heterogeneous EF with rGO-Fe_3O_4/CB@CF cathode was presented in Fig.3b. The concentration of SO_4^{2-} increased rapidly and accumulated until reaching the maximum value at 120 min indicating that the S bridge in the BSF molecule is a high reacting site for the attack of $^{\bullet}OH$ (Oturan et al., 2017). SO_4^{2-} concentration remained constant throughout the electrolysis (0.193 mM) corresponding to 97% of initial S atom.

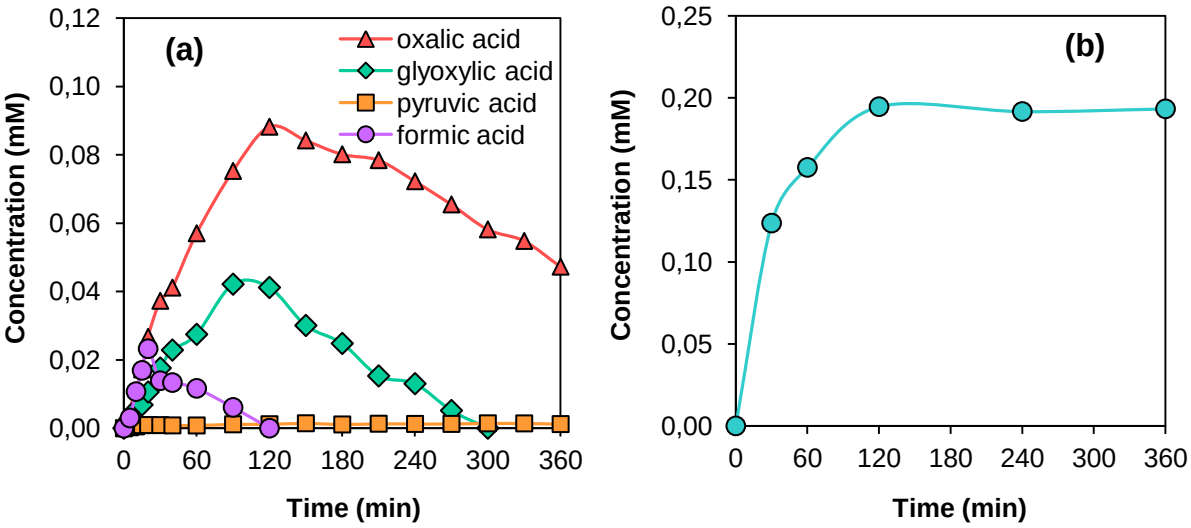

Fig. 3. Evolution of short-chain carboxylic acids **(a)** and sulfate ion **(b)** during heterogeneous EF treatment of 0.1 mM BSF solution (V = 80 mL) with BDD anode and rGO-Fe_3O_4/CB@CF cathode at pH=3. Applied current was 100 mA for carboxylic acids whereas it was 300 mA for inorganic ion. The supporting electrolyte was 50 mM Na_2SO_4 for carboxylic acids while it was 15 mM $NaClO_4$ for inorganic ions to avoid the interference of Na^+ and SO_4^{2-} ions on analysis.

3.5 Reaction pathway for the mineralization of BSF

Several organic by-products formed during EF treatment of BSF solution were identified by GC-MS and HPLC. Table SI-1 summarizes the characteristics of the

intermediates formed from oxidation of BSF. Based on these detected species, a reaction pathway (Fig.SI-7) is proposed for the mineralization of BSF by $^{\bullet}OH$. The intermediates I to IV were identified thanks to the fragmentation analysis of GC-MS spectrum while the intermediates V to VIII were identified by ion-exclusion HPLC analysis. The proposed pathway starts by the attack of $^{\bullet}OH$ on BSF leading to oxidative cleavage into molecules I and II. Compound III was resulted from hydroxylation of compound I, whereas compound IV was formed by the cyclization of compound via intramolecular alkylation (Feit and Rastrup-Andersen, 1973; Myers et al., 2017). The mineralization experiments led also to the formation of carboxylic acids (compounds V to VIII) (Fig.3a) and sulfate ion (Fig.3b), constituting the last stage of mineralization process.

3.6 Reusability of rGO-Fe_3O_4/CB@CF cathode

The stability of the cathode plays a crucial role in practical applications since it determines the reusability of the cathode in several runs without loss of activity. The reusability of the rGO-Fe_3O_4/CB@CF cathode was evaluated by repetitive experiments for mineralization of BSF (Fig.4). The electrode was gently rinsed with ultra-pure water and reused for the next cycle with identical conditions. The catalytic efficiency of the prepared cathode showed less than 4% reduction in terms of TOC removal after 3-h treatment for all five cycles, which shows the oxidation ability of multifunctional heterogeneous cathode and its advantage of avoiding iron leaching and therefore sludge formation. This result indicates that the rGO-Fe_3O_4/CB@CF cathode has great reusability and good stability at natural pH in consecutive operation conditions.

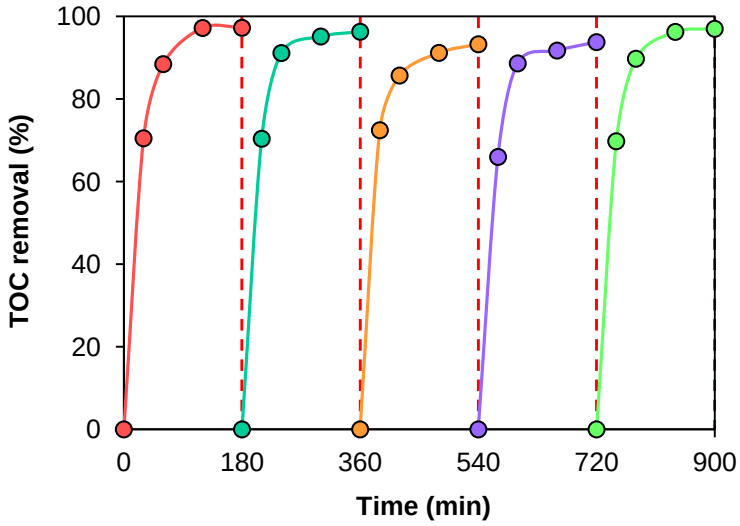

Fig. 4. Reusability of rGO-Fe_3O_4/CB@CF cathode for the TOC decay of BSF solution at the natural pH. [BSF] = 0.1 mM, I = 300 mA, [Na_2SO_4] = 50 mM, V = 80 mL

4. Conclusions

This study showed great ability of heterogeneous EF for efficient oxidation/mineralization of the cytostatic agent BSF. Excellent mineralization rate of BSF solutions was attained at 4 h electrolysis with 500 mA applied current for all configurations. It was verified that heterogeneous EF with modified cathodes and catalysts improved the mineralization of organic pollutants and widen the working pH range. Five cycle experiments proved that notable performance of heterogeneous EF with rGO-Fe_3O_4/CB@CF cathode for organic removal was achieved at natural pH of the solution with great stability. rGO-Fe_3O_4/CB@CF cathode played multiple roles in the heterogeneous EF process, it accelerated the ORR process to form the electro-generated H_2O_2, while activated the H_2O_2 simultaneously to form the $^{\bullet}OH$ radicals by means of heterogeneous EF process on its surface. Three heterogeneous EF configurations studied in this work provide three benefits over its homogeneous counterpart which could be a promising technique for the cost-effective and sustainable treatment: i) reusable cathode and catalyst, ii) ability to operate at natural pH, iii) improved cathodic properties leading to higher oxygen reduction activity. Formation and evolution of carboxylic acids and aromatic intermediates were also

assessed and based on identified intermediate products, a plausible mineralization pathway was proposed.

Author Contributions:

S.C.: Conceptualization, Investigation, Methodology, Draft preparation, Writing, Formal analysis.

B.Ö.: Conceptualization, Investigation, Validation, Writing

N.O.: Supervision, Methodology, Formal analysis

D.P.: Investigation, Formal analysis

C.T.: Supervision, Validation

M.A.O.: Supervision, Review & editing, Project administration

Acknowledgments: Sule Camcioglu and Baran Ozyurt acknowledge TUBITAK (The Scientific and Technological Research Council of Turkey) for providing financial support through 2219-International Postdoctoral Research Fellowship Program for Turkish Citizens. Sule Camcioglu and Baran Ozyurt thank both Ankara University and Gustave Eiffel University for their support of their postdoctoral research.

Conflicts of Interest: The authors declare no conflict of interest.

REFERENCES

Barhoumi, N., Olvera-Vargas, H., Oturan, N., Huguenot, D., Gadri, A., Ammar, S., Brillas, E., Oturan, M.A., 2017. Kinetics of oxidative degradation/mineralization pathways of the antibiotic tetracycline by the novel heterogeneous electro-Fenton process with solid catalyst chalcopyrite. Appl. Catal. B: Environ. 209, 637–647. https://doi.org/10.1016/j.apcatb.2017.03.034

Barhoumi, N., Oturan, N., Olvera-Vargas, H., Brillas, E., Gadri, A., Ammar, S., Oturan, M.A., 2016. Pyrite as a sustainable catalyst in electro-Fenton process for improving oxidation of sulfamethazine. Kinetics, mechanism and toxicity assessment. Water Res. 94, 52–61. https://doi.org/10.1016/j.watres.2016.02.042

Barışçı, S., Turkay, O., Ulusoy, E., Şeker, M.G., Yüksel, E., Dimoglo, A., 2018. Electro-oxidation of cytostatic drugs: Experimental and theoretical identification of by-products and evaluation of ecotoxicological effects. Chem. Eng. J. 334, 1820–1827. https://doi.org/10.1016/j.cej.2017.11.105

Berhe, R.N., Kassahun, S.K., Kang, J.W., Verma, M., Kim, H., 2022. Synthesis of Fe_3O_4/CNT/ACF cathode-based electro-fenton system for efficient mineralization of methylene blue dye: Kinetics and mechanism. J. Environ. Chem. Eng. 10, 108672. https://doi.org/10.1016/j.jece.2022.108672

Brillas, E., Martínez-Huitle, C.A., 2015. Decontamination of wastewaters containing synthetic organic dyes by electrochemical methods. An updated review. Appl. Catal. B: Environ. 166, 603–643. https://doi.org/10.1016/j.apcatb.2014.11.016

Brillas, E., Sirés, I., Oturan, M.A., 2009. Electro-Fenton Process and Related Electrochemical Technologies Based on Fenton's Reaction Chemistry. Chem. Rev. 109, 6570–6631. https://doi.org/10.1021/cr900136g

Burgos-Castillo, R.C., Sirés, I., Sillanpää, M., Brillas, E., 2018. Application of electrochemical advanced oxidation to bisphenol A degradation in water. Effect of sulfate and chloride ions. Chemosphere 194, 812–820. https://doi.org/10.1016/j.chemosphere.2017.12.014

Calza, P., Medana, C., Sarro, M., Rosato, V., Aigotti, R., Baiocchi, C., Minero, C., 2014. Photocatalytic degradation of selected anticancer drugs and identification of their transformation products in water by liquid chromatography–high resolution mass spectrometry. J. Chromatogr. A 1362, 135–144. https://doi.org/10.1016/j.chroma.2014.08.035

Camcioglu, S., Özyurt, B., Oturan, N., Trellu, C., Oturan, M.A., 2022. Fast and Complete Destruction of the Anti-Cancer Drug Cytarabine from Water by Electrocatalytic Oxidation Using Electro-Fenton Process. Catalysts 12, 1598. https://doi.org/10.3390/catal12121598

Cavalcante, R.P., da Rocha Sandim, L., Bogo, D., Barbosa, A.M.J., Osugi, M.E., Blanco, M., de Oliveira, S.C., de Fatima Cepa Matos, M., Machulek, A., Ferreira, V.S., 2013. Application of Fenton, photo-Fenton, solar photo-Fenton, and UV/H_2O_2 to degradation of the antineoplastic agent mitoxantrone and toxicological evaluation. Environ. Sci. Pollut. Res. 20, 2352–2361. https://doi.org/10.1007/s11356-012-1110-y

Chen, H., Zhang, Z., Yang, Z., Yang, Q., Li, B., Bai, Z., 2015. Heterogeneous fenton-like catalytic degradation of 2, 4-dichlorophenoxyacetic acid in water with FeS. Chem. Eng. J. 273, 481–489. https://doi.org/10.1016/j.cej.2015.03.079

Chen, L., Xie, J., Huang, L., Gong, X., 2023. Iron Oxide Anchored on Porous Carbon Derived from Metal–Organic Frameworks as an Efficient Catalyst toward In Situ Generation of H2O2 and a Hydroxyl Radical for Methylene Blue Degradation in Microbial Fuel Cells. Energy & Fuels 37, 5469–5477. https://doi.org/10.1021/acs.energyfuels.2c04185

Chen, W., Yang, X., Huang, J., Zhu, Y., Zhou, Y., Yao, Y., Li, C., 2016. Iron oxide containing graphene/carbon nanotube based carbon aerogel as an efficient E-Fenton cathode for the degradation of methyl blue. Electrochim. Acta 200, 75–83. https://doi.org/10.1016/j.electacta.2016.03.044

Cleveland, V., Bingham, J.-P., Kan, E., 2014. Heterogeneous Fenton degradation of bisphenol A by carbon nanotube-supported Fe_3O_4. Sep. Purif. Technol. 133, 388–395. https://doi.org/10.1016/j.seppur.2014.06.061

Coria, G., Pérez, T., Sirés, I., Brillas, E., Nava, J.L., 2018. Abatement of the antibiotic levofloxacin in a solar photoelectro-Fenton flow plant: modeling the dissolved organic carbon concentration-time relationship. Chemosphere 198, 174–181. https://doi.org/10.1016/j.chemosphere.2018.01.112

Cui, L., Li, Z., Li, Q., Chen, M., Jing, W., Gu, X., 2021. Cu/$CuFe_2O_4$ integrated graphite felt as a stable bifunctional cathode for high-performance heterogeneous electro-Fenton oxidation. Chem. Eng. J. 420, 127666. https://doi.org/10.1016/j.cej.2020.127666

Diaw, P.A., Oturan, N., Seye, M.D.G., Mbaye, O.M.A., Mbaye, M., Coly, A., Aaron, J.-

J., Oturan, M.A., 2020. Removal of the herbicide monolinuron from waters by the electro-Fenton treatment. J. Electroanal. Chem. 864, 114087. https://doi.org/10.1016/j.jelechem.2020.114087

Dos Santos, A.J., Sirés, I., Brillas, E., 2021. Removal of bisphenol A from acidic sulfate medium and urban wastewater using persulfate activated with electroregenerated Fe^{2+}. Chemosphere 263, 128271. https://doi.org/10.1016/j.chemosphere.2020.128271

Du, X., Oturan, M.A., Zhou, M., Belkessa, N., Su, P., Cai, J., Trellu, C., Mousset, E., 2021. Nanostructured electrodes for electrocatalytic advanced oxidation processes: From materials preparation to mechanisms understanding and wastewater treatment applications. Appl. Catal. B: Environ. 296, 120332. https://doi.org/https://doi.org/10.1016/j.apcatb.2021.120332

Feit, P.W., Rastrup-Andersen, N., 1973. 4-Methanesulfonyloxybutanol: hydrolysis of busulfan. J. Pharm. Sci. 62, 1007–1008.

Feng, L., Song, W., Oturan, N., Karbasi, M., van Hullebusch, E.D., Esposito, G., Giannakis, S., Oturan, M.A., 2023. Electrochemical oxidation of Naproxen in aqueous matrices: Elucidating the intermediates' eco-toxicity, by assessing its degradation pathways via experimental and density functional theory (DFT) approaches. Chem. Eng. J. 451, 138483. https://doi.org/10.1016/j.cej.2022.138483

Ganiyu, S.O., Nidheesh, P.V., Oturan, M.A., 2022. Synthesis and application of nanostructured iron oxides heterogeneous catalysts for environmental applications, in: Advanced Materials for Sustainable Environmental Remediation. Elsevier, pp. 583–608. https://doi.org/10.1016/B978-0-323-90485-8.00014-X

Ganiyu, S.O., Zhou, M., Martínez-Huitle, C.A., 2018. Heterogeneous electro-Fenton and photoelectro-Fenton processes: a critical review of fundamental principles and application for water/wastewater treatment. Appl. Catal. B: Environ. 235, 103–129. https://doi.org/10.1016/j.apcatb.2018.04.044

Gao, L., Zhuang, J., Nie, L., Zhang, J., Zhang, Y., Gu, N., Wang, T., Feng, J., Yang, D., Perrett, S., 2007. Intrinsic peroxidase-like activity of ferromagnetic nanoparticles. Nat. Nanotechnol. 2, 577–583. https://doi.org/10.1038/nnano.2007.260

Garcia-Segura, S., Brillas, E., 2011. Mineralization of the recalcitrant oxalic and oxamic acids by electrochemical advanced oxidation processes using a boron-doped diamond anode. Water Res. 45, 2975–2984.

https://doi.org/10.1016/j.watres.2011.03.017

Geraldino, H.C.L., Freitas, T.K.F.S., Manholer, D.D., França, F., Oliveira, J.H., Volnistem, E.A., Lima, A.R.F., Bertotti, M., Girotto, E.M., Garcia, J.C., 2020. Electrochemical generation of H_2O_2 using gas diffusion electrode improved with rGO intensified with the Fe_3O_4/GO catalyst for degradation of textile wastewater. J. Water Process Eng. 36, 101377. https://doi.org/10.1016/j.jwpe.2020.101377

González-Burciaga, L.A., García-Prieto, J.C., García-Roig, M., Lares-Asef, I., Núñez-Núñez, C.M., Proal-Nájera, J.B., 2021. Cytostatic drug 6-mercaptopurine degradation on pilot scale reactors by advanced oxidation processes: UV-C/H_2O_2 and UV-C/TiO_2/H_2O_2 kinetics. Catalysts 11, 567. https://doi.org/10.3390/catal11050567

González-Burciaga, L.A., Núñez-Núñez, C.M., Proal-Nájera, J.B., 2022. Challenges of TiO_2 heterogeneous photocatalysis on cytostatic compounds degradation: State of the art. Environ. Sci. Pollut. Res. 29, 42251–42274. https://doi.org/10.1007/s11356-021-17241-8

Gopinath, A., Pisharody, L., Popat, A., Nidheesh, P. V, 2022. Supported catalysts for heterogeneous electro-Fenton processes: Recent trends and future directions. Curr. Opin. Solid State Mater. Sci. 26, 100981. https://doi.org/https://doi.org/10.1016/j.cossms.2022.100981

Görmez, F., Görmez, Ö., Gözmen, B., Kalderis, D., 2019. Degradation of chloramphenicol and metronidazole by electro-Fenton process using graphene oxide-Fe3O4 as heterogeneous catalyst. J. Environ. Chem. Eng. 7, 102990. https://doi.org/10.1016/j.jece.2019.102990

Governo, M., Santos, M.S.F., Alves, A., Madeira, L.M., 2017. Degradation of the cytostatic 5-Fluorouracil in water by Fenton and photo-assisted oxidation processes. Environ. Sci. Pollut. Res. 24, 844–854. https://doi.org/10.1007/s11356-016-7827-2

Hien, S.A., Trellu, C., Oturan, N., Assémian, A.S., Briton, B.G.H., Drogui, P., Adouby, K., Oturan, M.A., 2022. Comparison of homogeneous and heterogeneous electrochemical advanced oxidation processes for treatment of textile industry wastewater. J. Hazard. Mater. 129326. https://doi.org/10.1016/j.jhazmat.2022.129326

Houot, M., Poinsignon, V., Mercier, L., Valade, C., Desmaris, R., Lemare, F., Paci, A., 2013. Physico-chemical stability of busulfan in injectable solutions in various

administration packages. Drugs R. D. 13, 87–94. https://doi.org/10.1007/s40268-013-0003-y

Hua, Z., Ma, W., Bai, X., Feng, R., Yu, L., Zhang, X., Dai, Z., 2014. Heterogeneous Fenton degradation of bisphenol A catalyzed by efficient adsorptive Fe_3O_4/GO nanocomposites. Environ. Sci. Pollut. Res. 21, 7737–7745. https://doi.org/10.1007/s11356-014-2728-8

Ioannou-Ttofa, L., Fatta-Kassinos, D., 2020. Cytostatic drug residues in wastewater treatment plants: Sources, removal efficiencies and current challenges. Fate Eff. Anticancer Drugs Environ. 103–138. https://doi.org/10.1007/978-3-030-21048-9_6

Kanjal, M.I., Muneer, M., Abdelhaleem, A., Chu, W., 2020. Degradation of methotrexate by UV/peroxymonosulfate: Kinetics, effect of operational parameters and mechanism. Chinese J. Chem. Eng. 28, 2658–2667. https://doi.org/10.1016/j.cjche.2020.05.033

Kosjek, T., Negreira, N., Heath, E., de Alda, M.L., Barceló, D., 2018. Aerobic activated sludge transformation of vincristine and identification of the transformation products. Sci. Total Environ. 610, 892–904. https://doi.org/10.1016/j.scitotenv.2017.08.061

Kulaksız, E., Kayan, B., Gözmen, B., Kalderis, D., Oturan, N., Oturan, M.A., 2022. Comparative degradation of 5-fluorouracil in aqueous solution by using H_2O_2-modified subcritical water, photocatalytic oxidation and electro-Fenton processes. Environ. Res. 204, 111898. https://doi.org/10.1016/j.envres.2021.111898

Le, T.X.H., Bechelany, M., Lacour, S., Oturan, N., Oturan, M.A., Cretin, M., 2015. High removal efficiency of dye pollutants by electron-Fenton process using a graphene based cathode. Carbon N. Y. 94, 1003–1011. https://doi.org/10.1016/j.carbon.2015.07.086

Li, J., Ai, Z., Zhang, L., 2009. Design of a neutral electro-Fenton system with Fe@ Fe_2O_3/ACF composite cathode for wastewater treatment. J. Hazard. Mater. 164, 18–25. https://doi.org/10.1016/j.jhazmat.2008.07.109

Li, W., Nanaboina, V., Chen, F., Korshin, G. V, 2016. Removal of polycyclic synthetic musks and antineoplastic drugs in ozonated wastewater: quantitation based on the data of differential spectroscopy. J. Hazard. Mater. 304, 242–250. https://doi.org/10.1016/j.jhazmat.2015.10.035

Lin, H., Oturan, N., Wu, J., Zhang, H., Oturan, M.A., 2017. Cold incineration of sucralose in aqueous solution by electro-Fenton process. Sep. Purif. Technol.

173, 218–225. https://doi.org/10.1016/j.seppur.2016.09.028

Márquez, A.A., Sirés, I., Brillas, E., Nava, J.L., 2020. Mineralization of Methyl Orange azo dye by processes based on H_2O_2 electrogeneration at a 3D-like air-diffusion cathode. Chemosphere 259, 127466. https://doi.org/10.1016/j.chemosphere.2020.127466

Martínez-Huitle, C.A., Einaga, Y., Oturan, M.A., 2022. Conductive-synthetic diamond materials in meeting the sustainable development goals. Curr. Opin. Solid State Mater. Sci. 26, 101019. https://doi.org/https://doi.org/10.1016/j.cossms.2022.101019

Martínez-Huitle, C.A., Rodrigo, M.A., Sirés, I., Scialdone, O., 2023. A critical review on latest innovations and future challenges of electrochemical technology for the abatement of organics in water. Appl. Catal. B: Environ. 328, 122430. https://doi.org/https://doi.org/10.1016/j.apcatb.2023.122430

Mbaye, M., Diaw, P.A., Mbaye, O.M.A., Oturan, N., Seye, M.D.G., Trellu, C., Coly, A., Tine, A., Aaron, J.-J., Oturan, M.A., 2022. Rapid removal of fungicide thiram in aqueous medium by electro-Fenton process with Pt and BDD anodes. Sep. Purif. Technol. 281, 119837. https://doi.org/10.1016/j.seppur.2021.119837

Moratalla, Á., Lacasa, E., Cañizares, P., Rodrigo, M.A., Sáez, C., 2022. Electro-Fenton-based technologies for selectively degrading antibiotics in aqueous media. Catalysts 12, 602. https://doi.org/10.3390/catal12060602

Murrieta, M.F., Sirés, I., Brillas, E., Nava, J.L., 2020. Mineralization of Acid Red 1 azo dye by solar photoelectro-Fenton-like process using electrogenerated HClO and photoregenerated Fe(II). Chemosphere 246, 125697. https://doi.org/10.1016/j.chemosphere.2019.125697

Muzenda, C., Arotiba, O.A., 2022. Improved magnetite nanoparticle immobilization on a carbon felt cathode in the heterogeneous electro-Fenton degradation of aspirin in wastewater. ACS omega 7, 19261–19269. https://doi.org/10.1021/acsomega.2c00627

Myers, A.L., Kawedia, J.D., Champlin, R.E., Kramer, M.A., Nieto, Y., Ghose, R., Andersson, B.S., 2017. Clarifying busulfan metabolism and drug interactions to support new therapeutic drug monitoring strategies: a comprehensive review. Expert Opin. Drug Metab. Toxicol. 13, 901–923. https://doi.org/10.1080/17425255.2017.1360277

Nidheesh, P.V., Ganiyu, S.O., Martínez-Huitle, C.A., Mousset, E., Olvera-Vargas, H.,

Trellu, C., Zhou, M., Oturan, M.A., 2023a. Recent advances in electro-Fenton process and its emerging applications. Crit. Rev. Environ. Sci. Technol. 53, 887–913. https://doi.org/10.1080/10643389.2022.2093074

Nidheesh, P.V., Trellu, C., Vargas, H.O., Mousset, E., Ganiyu, S.O., Oturan, M.A., 2023b. Electro-Fenton process in combination with other advanced oxidation processes: Challenges and opportunities. Curr. Opin. Electrochem. 37, 101171. https://doi.org/https://doi.org/10.1016/j.coelec.2022.101171

Olvera-Vargas, H., Wang, Z., Xu, J., Lefebvre, O., 2022. Synergistic degradation of GenX (hexafluoropropylene oxide dimer acid) by pairing graphene-coated Ni-foam and boron doped diamond electrodes. Chem. Eng. J. 430, 132686. https://doi.org/https://doi.org/10.1016/j.cej.2021.132686

Oturan, N., Ganiyu, S.O., Raffy, S., Oturan, M.A., 2017. Sub-stoichiometric titanium oxide as a new anode material for electro-Fenton process: Application to electrocatalytic destruction of antibiotic amoxicillin. Appl. Catal. B: Environ. 217, 214–223. https://doi.org/10.1016/j.apcatb.2017.05.062

Poza-Nogueiras, V., Rosales, E., Pazos, M., Sanroman, M.A., 2018. Current advances and trends in electro-Fenton process using heterogeneous catalysts–a review. Chemosphere 201, 399–416. https://doi.org/10.1016/j.chemosphere.2018.03.002

Roig, B., Marquenet, B., Delpla, I., Bessonneau, V., Sellier, A., Leder, C., Thomas, O., Bolek, R., Kummerer, K., 2014. Monitoring of methotrexate chlorination in water. Water Res. 57, 67–75. https://doi.org/10.1016/j.watres.2014.03.008

Rusevova, K., Kopinke, F.-D., Georgi, A., 2012. Nano-sized magnetic iron oxides as catalysts for heterogeneous Fenton-like reactions—Influence of Fe (II)/Fe (III) ratio on catalytic performance. J. Hazard. Mater. 241, 433–440. https://doi.org/10.1016/j.jhazmat.2012.09.068

Sadeghi, M., Mehdinejad, M.H., Mengelizadeh, N., Mahdavi, Y., Pourzamani, H., Hajizadeh, Y., Zare, M.R., 2019. Degradation of diclofenac by heterogeneous electro-Fenton process using magnetic single-walled carbon nanotubes as a catalyst. J. Water Process Eng. 31, 100852. https://doi.org/10.1016/j.jwpe.2019.100852

Scaria, J., Nidheesh, P.V., 2022. Magnetite–reduced graphene oxide nanocomposite as an efficient heterogeneous Fenton catalyst for the degradation of tetracycline antibiotics. Environ. Sci. Water Res. Technol. 8, 1261–1276.

https://doi.org/10.1039/D2EW00019A

Sellers, R.M., 1980. Spectrophotometric determination of hydrogen peroxide using potassium titanium (IV) oxalate. Analyst 105, 950–954. https://doi.org/10.1016/j.saa.2019.117138

Siedlecka, E.M., 2020. Removal of cytostatic drugs from water and wastewater: Progress in the development of advanced treatment methods. Fate Eff. Anticancer drugs Environ. 197–219. https://doi.org/10.1007/978-3-030-21048-9_9

Sirés, I., Brillas, E., Oturan, M.A., Rodrigo, M.A., Panizza, M., 2014. Electrochemical advanced oxidation processes: today and tomorrow. A review. Environ. Sci. Pollut. Res. 21, 8336–8367. https://doi.org/10.1007/s11356-014-2783-1

Skoglund, C., Bassyouni, F., Abdel-Rehim, M., 2013. Monolithic packed 96-tips set for high-throughput sample preparation: determination of cyclophosphamide and busulfan in whole blood samples by monolithic packed 96-tips and LC-MS. Biomed. Chromatogr. 27, 714–719. https://doi.org/10.1016/j.chroma.2009.10.072

Sopaj, F., Oturan, N., Pinson, J., Podvorica, F.I., Oturan, M.A., 2020. Effect of cathode material on electro-Fenton process efficiency for electrocatalytic mineralization of the antibiotic sulfamethazine. Chem. Eng. J. 384, 331–341. https://doi.org/10.1016/j.cej.2019.123249

Wang, Yujing, Zhao, G., Chai, S., Zhao, H., Wang, Yanbin, 2013. Three-dimensional homogeneous ferrite-carbon aerogel: one pot fabrication and enhanced electro-Fenton reactivity. ACS Appl. Mater. Interfaces 5, 842–852. https://doi.org/10.1021/am302437a

Xie, F., Gao, Y., Zhang, Jingbin, Bai, H., Zhang, Jianfeng, Li, Z., Zhu, W., 2022. A novel bifunctional cathode for the generation and activation of H_2O_2 in electro-Fenton: characteristics and mechanism. Electrochim. Acta 430, 141099. https://doi.org/10.1016/j.electacta.2022.141099

Xu, L., Wang, J., 2012. Fenton-like degradation of 2, 4-dichlorophenol using Fe_3O_4 magnetic nanoparticles. Appl. Catal. B: Environ. 123, 117–126. https://doi.org/10.1016/j.apcatb.2012.04.028

Xue, X., Hanna, K., Deng, N., 2009. Fenton-like oxidation of Rhodamine B in the presence of two types of iron (II, III) oxide. J. Hazard. Mater. 166, 407–414. https://doi.org/10.1016/j.apcatb.2012.04.028

Yang, W., Oturan, N., Raffy, S., Zhou, M., Oturan, M.A., 2020a. Electrocatalytic generation of homogeneous and heterogeneous hydroxyl radicals for cold

mineralization of anti-cancer drug Imatinib. Chem. Eng. J. 383. https://doi.org/10.1016/j.cej.2019.123155

Yang, W., Zhou, M., Cai, J., Liang, L., Ren, G., Jiang, L., 2017. Ultrahigh yield of hydrogen peroxide on graphite felt cathode modified with electrochemically exfoliated graphene. J. Mater. Chem. A 5, 8070–8080. https://doi.org/10.1039/C7TA01534H

Yang, W., Zhou, M., Oturan, N., Bechelany, M., Cretin, M., Oturan, M.A., 2020b. Highly efficient and stable FeIIFeIII LDH carbon felt cathode for removal of pharmaceutical ofloxacin at neutral pH. J. Hazard. Mater. 393, 122513. https://doi.org/10.1016/j.jhazmat.2020.122513

Yang, W., Zhou, M., Oturan, N., Li, Y., Oturan, M.A., 2019. Electrocatalytic destruction of pharmaceutical imatinib by electro-Fenton process with graphene-based cathode. Electrochim. Acta 305, 285–294. https://doi.org/https://doi.org/10.1016/j.electacta.2019.03.067

Yu, L., Yang, X., Ye, Y., Wang, D., 2015. Efficient removal of atrazine in water with a Fe 3 O 4/MWCNTs nanocomposite as a heterogeneous Fenton-like catalyst. RSC Adv. 5, 46059–46066. https://doi.org/10.1039/C5RA04249F

Zhang, J., Chang, V.W.C., Giannis, A., Wang, J.-Y., 2013. Removal of cytostatic drugs from aquatic environment: a review. Sci. Total Environ. 445, 281–298. https://doi.org/10.1016/j.scitotenv.2012.12.061

Zhang, J., Wang, G., Zhang, L., Fu, X., Liu, Y., 2014. Catalytic oxidative desulfurization of benzothiophene with hydrogen peroxide catalyzed by Fenton-like catalysts. React. Kinet. Mech. Catal. 113, 347–360. https://doi.org/10.1007/s11144-014-0750-y

Zhao, H., Wang, Yujing, Wang, Yanbin, Cao, T., Zhao, G., 2012. Electro-Fenton oxidation of pesticides with a novel Fe_3O_4@ Fe_2O_3/activated carbon aerogel cathode: High activity, wide pH range and catalytic mechanism. Appl. Catal. B: Environ. 125, 120–127. https://doi.org/10.1016/j.apcatb.2012.05.044

Zhou, L., Zhang, H., Ji, L., Shao, Y., Li, Y., 2014. Fe_3O_4/MWCNT as a heterogeneous Fenton catalyst: degradation pathways of tetrabromobisphenol A. Rsc Adv. 4, 24900–24908. https://doi.org/10.1039/C4RA02333A

Zhou, Y., Liu, X., Zhao, Y., Luo, S., Wang, L., Yang, Y., Oturan, M.A., Mu, Y., 2018. Structure-based synergistic mechanism for the degradation of typical antibiotics in electro-Fenton process using Pd–Fe_3O_4 model catalyst: Theoretical and

experimental study. J. Catal. 365, 184–194. https://doi.org/10.1016/j.jcat.2018.07.006

Zubir, N.A., Yacou, C., Motuzas, J., Zhang, X., Zhao, X.S., da Costa, J.C.D., 2015. The sacrificial role of graphene oxide in stabilising a Fenton-like catalyst GO–Fe_3O_4. Chem. Commun. 51, 9291–9293. https://doi.org/10.1039/C5CC02292D